Acta Crystallographica Section D
Biological Crystallography
ISSN 0907-4449

X-ray structure of a soluble Rieske-type ferredoxin from *Mus musculus*

Elena J. Levin,[a] Nathaniel L. Elsen,[a] Kory D. Seder,[b] Jason G. McCoy,[a] Brian G. Fox[a,b] and George N. Phillips Jr[a,b]*

[a]Department of Biochemistry, University of Wisconsin, Madison, USA, and [b]Center for Eukaryotic Structural Genomics, University of Wisconsin, Madison, USA

Correspondence e-mail: phillips@biochem.wisc.edu

Received 29 May 2008
Accepted 11 July 2008

PDB Reference: Rieske-type ferredoxin, 3d89, r3d89sf.

The 2.07 Å resolution X-ray crystal structure of a soluble Rieske-type ferredoxin from *Mus musculus* encoded by the gene Mm.266515 is reported. Although they are present as covalent domains in eukaryotic membrane oxidase complexes, soluble Rieske-type ferredoxins have not previously been observed in eukaryotes. The overall structure of the mouse Rieske-type ferredoxin is typical of this class of iron–sulfur proteins and consists of a larger partial β-barrel domain and a smaller domain containing Cys57, His59, Cys80 and His83 that binds the [2Fe–2S] cluster. The S atoms of the cluster are hydrogen-bonded by six backbone amide N atoms in a pattern typical of membrane-bound high-potential eukaryotic respiratory Rieske ferredoxins. However, phylogenetic analysis suggested that the mouse Rieske-type ferredoxin was more closely related to bacterial Rieske-type ferredoxins. Correspondingly, the structure revealed an extended loop most similar to that seen in Rieske-type ferredoxin subunits of bacterial aromatic dioxygenases, including the positioning of an aromatic side chain (Tyr85) between this loop and the [2Fe–2S] cluster. The mouse Rieske-type ferredoxin was shown to be capable of accepting electrons from both eukaryotic and prokaryotic oxidoreductases, although it was unable to serve as an electron donor for a bacterial monooxygenase complex. The human homolog of mouse Rieske-type ferredoxin was also cloned and purified. It behaved identically to mouse Rieske-type ferredoxin in all biochemical characterizations but did not crystallize. Based on its high sequence identity, the structure of the human homolog is likely to be modeled well by the mouse Rieske-type ferredoxin structure.

1. Introduction

Rieske ferredoxins were originally identified by an unusual EPR signal in beef heart mitochondria preparations (Rieske, 1968). They are now well characterized as containing two Fe atoms and two bridging S atoms arranged in a tetrahedral rhombus, with one iron coordinated by the ND1 atoms of two histidine residues and the other iron coordinated by the SG atoms of two cysteine residues. In the oxidized [2Fe–2S] cluster both Fe atoms carry charges of 3+, while in the reduced form the iron coordinated by two histidines assumes the 2+ state (Fee *et al.*, 1984; Iwata *et al.*, 1996).

Although the fold of the various Rieske and Rieske-type ferredoxins is well conserved, their sequence identity is low. Only the four residues coordinating the cluster are absolutely

conserved and these are arranged in a C*X*H and C*XX*H metal-binding motif separated by a variable sequence of typically not less than 15 residues (Schmidt & Shaw, 2001). Other amino-acid positions in these ubiquitously distributed proteins have diverged extensively.

Rieske ferredoxins are involved in a wide variety of biological functions. They typically act as electron carriers between different redox partners. Membrane-bound Rieske ferredoxins are found as covalent domains in the cytochrome bc_1, b_6f and *bc* respiratory complexes in mitochondria, chloroplasts and bacterial cell walls (Trumpower & Gennis, 1994), as well as in the respiratory chains of archaeal organisms (Schafer *et al.*, 1996). In bacteria, Rieske-type ferredoxins are found in tightly bound subunits of arsenite oxidase (Ellis *et al.*, 2001), nitrite reductases (Lledo *et al.*, 2004) and the oxygenase components of various aromatic ring-hydroxylating monooxygenases and dioxygenases (Ferraro *et al.*, 2005). Rieske-type ferredoxins also participate as soluble electron carriers in some bacterial monooxygenases and dioxygenases. In mammals, proteins previously observed to contain Rieske [2Fe–2S] clusters include CMP-*N*-acetylneuraminic acid hydroxylase (Schlenzka *et al.*, 1996) and a protein homologous to apoptosis-inducing factor, the Rieske domain of which has been shown to induce apoptosis in human cell cultures (Xie *et al.*, 2005).

As part of our application of structural genomics methods to eukaryotic proteins, we investigated the proteins encoded by the mouse gene Mm.266515 and its human homolog Hs.BC024023. Here, we describe the cloning and purification of previously uncharacterized soluble Rieske-type ferredoxins from *Mus musculus* (MRF) and *Homo sapiens* (HRF) of unknown function and the determination of the X-ray structure of MRF to 2.07 Å. The function of these proteins is presently unknown. However, the crystal structure exhibits a high degree of similarity to the structures of the bacterial Rieske ferredoxin domains of various aromatic oxygenase complexes (Kauppi *et al.*, 1998; Colbert *et al.*, 2000; Moe *et al.*, 2006; Nam *et al.*, 2005). In addition, we demonstrate that MRF and HRF can be reduced chemically by dithionite and biologically by both prokaryotic and eukaryotic oxidoreductases.

2. Methods

2.1. Materials

Unless otherwise noted, all materials were purchased from Sigma–Aldrich (St Louis, Missouri, USA). The cDNA containing the Mm.266515 gene was purchased from Open Biosystems (Huntsville, Alabama, USA).

2.2. Cloning and expression

The gene Mm.266515 encoding MRF or Hs.BC024023 encoding HRF was cloned into expression plasmid pVP16 to allow production of the protein as an N-terminal fusion to His_8-maltose-binding protein (Thao *et al.*, 2004). *Escherichia coli* BL21 transformed with the plasmid containing the target gene was grown in 4 l Erlenmeyer flasks containing 1 l Luria–Bertani medium modified by the addition of 50 m*M* phosphate buffer pH 6.7 containing 50 m*M* NH_4Cl, 5 m*M* Na_2SO_4 and 100 µg ml^{-1} ampicillin. Expression was induced by the addition of IPTG (10 µ*M* final concentration), L-cysteine (1 m*M* final concentration), $Fe(NH_4)_2(SO_4)_2$ (100 µ*M* final concentration), 1 g l^{-1} casamino acids and 0.4%(*w*/*v*) glycerol when the shaken flask culture reached an OD_{600} of ∼0.4. After induction, the culture was grown overnight (∼14 h) at 303 K.

2.3. Protein purification

All protein-purification steps were performed at 277 K. 2 ml buffer *A* (25 m*M* MOPS pH 7.4 containing 200 m*M* NaCl and 1 m*M* dithiothreitol) was added per gram of frozen cell paste. The resuspended cells were amended with 1 mg each of RNAse, DNAse and lysozyme and lysed by sonication. After sonication, the lysed cells were further diluted with 2 ml buffer *A* per gram of cell paste and centrifuged at 40 000*g* for 1 h. The supernatant was loaded onto a 45 ml amylose column equilibrated in buffer *A*. The column was washed with five column volumes of buffer *A*. The bound protein was batch-eluted with one column volume of buffer *A* containing 10 m*M* maltose. Tobacco etch virus (TEV) protease was added to the eluted protein to a concentration of 1 g per 100 g of total protein and allowed to react overnight. The net result of fusion to MBP followed by cleavage by TEV protease was the replacement of the N-terminal methionine by serine. The solution was then concentrated to 4 ml and loaded onto a 16/60 Sephadex S-100 gel-filtration column (GE Healthcare, Piscataway, New Jersey, USA) equilibrated in buffer *B* [25 m*M* MOPS pH 7.2 containing 100 m*M* NaCl, 7%(*w*/*v*) glycerol, 5 m*M* maltose and 1 m*M* dithiothreitol]. Fractions containing MRF were pooled based on the presence of an optical absorption spectrum typical of an iron–sulfur protein, concentrated and dialyzed into crystallization buffer (10 m*M* MOPS pH 7.0 containing 25 m*M* NaCl). The final protein concentration was measured by Bradford assay.

2.4. Crystallization and data collection

The purified MRF was crystallized by hanging-drop vapor diffusion at 293 K with a reservoir solution consisting of 120 m*M* trisodium citrate, 100 m*M* MES pH 6.0–6.5 and 22–25% PEG MME 5000. The drops contained 2 µl reservoir solution and 2 µl protein solution, resulting in the initial drop having a protein concentration of ∼7.5 mg ml^{-1}. The resulting crystals were deep red octahedrons roughly 75 × 75 × 100 µm in size. After soaking for approximately 3 min in cryoprotectant consisting of the reservoir solution plus 15% ethylene glycol, the crystals were flash-frozen in liquid N_2. In addition to the native crystals, mercury derivatives were prepared by soaking the crystals overnight in solutions of mother liquor with 2 m*M* thimerosal added. Diffraction data were collected from a single mercury-derivatized crystal on the Southeast Regional Collaborative Access Team beamline 22-ID at the Advanced Photon Source at a wavelength of 1.0 Å to a nominal resolution of 1.7 Å. An additional data set was collected on a crystal of the native protein to a resolution of

2.07 Å at the General Medicine and Cancer Institutes Collaborative Access Team beamline 23-ID-D using a wavelength of 0.964 Å. Both data sets were indexed and scaled using *HKL*-2000 (Otwinowski & Minor, 1997).

2.5. Phasing and structure solution

The programs *HySS* from the *Phenix* suite (Adams *et al.*, 2002) and *SHELXD* (Sheldrick, 2008) were used to locate four Hg atoms in the asymmetric unit of the thimerosal-derivatized crystal. The structure was phased using the program *autoSHARP* (Vonrhein *et al.*, 2006) and an initial model was built using *ARP*/*wARP* (Cohen *et al.*, 2004). Model building and refinement were continued using *Coot* (Emsley & Cowtan, 2004) and *REFMAC* (Murshudov *et al.*, 1997; Winn *et al.*, 2001) until 137 residues had been located and R and $R_{\rm free}$ were 19.8% and 24.1%, respectively. The resulting model was then used to obtain phases for the 2.07 Å native data set by molecular replacement in *MOLREP* (Vagin & Teplyakov, 1997). After additional model building and TLS refinement using TLS groups determined by the program *TLSMD* (Painter & Merritt, 2006), the geometry of the final model was assessed using *MOLPROBITY* (Davis *et al.*, 2007).

2.6. Reductive titrations

For studies of sodium dithionite reduction, 90 µ*M* MRF was made anaerobic in a sealed quartz cuvette by repeated cycles of vacuum/argon. Reductant (a concentrated solution of sodium dithionite quantified by reductive titration of potassium ferricyanide) was added in 1 µl aliquots using a gas-tight syringe. The optical spectrum of MRF was monitored using a Hewlett Packard 8453 diode array spectrophotometer. Reduction rates were measured similarly, except that T4moF, a prokaryotic oxidoreductase, was included in the anaerobic cuvette at 4 n*M*. Anaerobic NADH was then added to a final concentration of 1 m*M*. The rate was calculated from the initial linear decrease in absorbance at 460 nm.

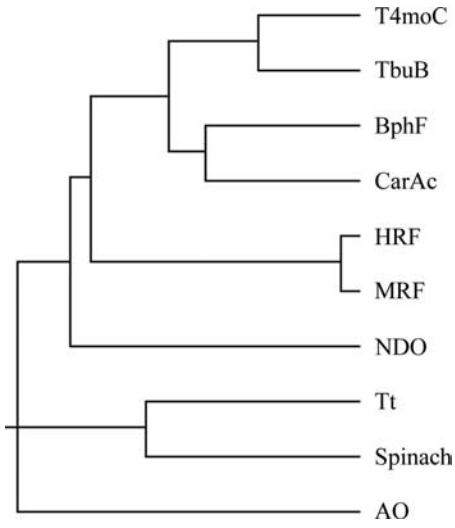

Figure 1
Phylogenetic tree constructed based on a structure-edited alignment of Rieske protein sequences.

2.7. Other methods

The total iron content was measured by the tripyridyl-*S*-triazine assay (Fischer & Price, 1964). Rieske ferredoxin sequences were aligned and a phylogenetic tree was constructed using *MegAlign* (Clewley & Arnold, 1997). The amino-acid sequences of multisubunit enzymes were trimmed to the Rieske domain. The resulting sequence-based alignment was then edited based on the backbone alignment of the crystal structures using the align routine in *PyMOL* (DeLano Scientific LLC, San Carlos, California, USA). Electrostatic surface calculations were performed using the *APBS Tools* plugin for *PyMOL* (Baker *et al.*, 2001).

3. Results and discussion

3.1. Phylogenetic analysis

Fig. 1 shows a phylogenetic tree of some Rieske proteins and Rieske-type ferredoxins from a variety of species. T4moC and TbuB are soluble Rieske-type ferredoxins that function as electron carriers to bacterial multicomponent monooxygenases (Leahy *et al.*, 2003). BphF and CarAc are also soluble bacterial Rieske-type ferredoxins, but they transfer electrons to Rieske nonheme iron oxygenases (ROs; Colbert *et al.*, 2000; Nam *et al.*, 2005). Naphthalene dioxygenase (NDO) is an RO, the Rieske domain of which has been used in the sequence alignment (Kauppi *et al.*, 1998). The *Thermus thermophilus* (Tt) and spinach Rieske proteins are membrane-tethered and function in chemiosmotic respiratory complexes (Hunsicker-Wang *et al.*, 2003; Carrell *et al.*, 1997). The enzyme arsenite oxidase (AO) from *Alcaligenes faecalis* is a molybdenum/iron protein involved in the detoxification of arsenic and contains a 133-amino-acid Rieske subunit (Ellis *et al.*, 2001).

Homologs to MRF are present in the genome sequences of other vertebrate animals and the human homolog (HRF) is included in the phylogenetic tree. Interestingly, this protein clade is more closely related to the prokaryotic soluble Rieske-type ferredoxins than the membrane-bound Rieske proteins found in the respiratory complexes of eukaryotes.

3.2. Expression and purification

Overnight induction of cells transformed with the MRF expression plasmid yielded ∼6 g per litre of wet cell paste. Overnight induction with 10 µ*M* IPTG resulted in an expression level of between 10% and 20% of the total cellular protein. Higher expression levels could be achieved with higher IPTG concentrations (>40% of the total protein), but this always resulted in lower [2Fe–2S] cluster incorporation. The expressed fusion protein was purified to >95% purity by a two-step purification consisting of an amylose resin affinity-chromatography step and a gel-filtration step. The MRF, with a calculated molecular weight of 18 kDa, was not separated from the His_8-MBP fragment (∼46 kDa) using gel-filtration chromatography unless maltose was included in the column buffer. This is likely to be the consequence of a conforma-

Table 1
Data-collection and refinement statistics.

A summary of crystal and data-collection statistics for the thimerosal-derivatized crystals and refinement statistics for the corresponding models. Values in parentheses are for the highest resolution shell (1.69–1.73 Å for the derivative data set and 2.07–2.14 Å for the native data set).

	Thimerosal derivative	Native
Data collection		
Space group	$P4_32_12$	$P4_32_12$
Unit-cell parameters (Å)	a = 52.67, c = 108.01	a = 52.41, c = 108.81
Wavelength (Å)	1.00	0.964
Resolution (Å)	1.69	2.07
Unique reflections	16626	9282
Completeness (%)	98.7 (90.2)	99.4 (95.5)
$I/\sigma(I)$	12.9 (1.33)	18.4 (1.84)
R_{merge} (%)	17.6	5.7
Refinement		
No. of TLS groups†	5	4
R factor (%)	19.8 (25.7)	19.9 (29.5)
R_{free} (%)	24.1 (37.6)	22.8 (37.8)
Bond r.m.s.d. (Å)	0.017	0.019
Angle r.m.s.d. (°)	1.820	1.848
PDB code	—	3d89

† For the thimerosal-deriviatized structure, the TLS groups covered residues 13–36, 37–55, 56–93, 94–119 and 120–148. In the native structure, the four TLS groups covered residues 14–18, 19–35, 36–133 and 134–154.

tional change of MBP upon binding maltose (Sharff *et al.*, 1992) which causes an altered elution pattern.

The purified MRF had a distinctive red–brown color and the optical absorbance spectrum showed peaks at 330 and 460 nm with molar absorptivity constants of 6000 and 11 600 M^{-1} cm^{-1}, respectively, and a shoulder at 570 nm. This spectrum is typical of a Rieske ferredoxin (Fig. 2). The iron content of the purified protein was only 45% of that expected, indicating incomplete [2Fe–2S] cofactor incorporation during expression in the exogenous host or partial loss during the purification procedure. Expression and purification of HRF following the same protocol resulted in similar purity and [2Fe–2S] cofactor incorporation; however, HRF had an increased tendency to form high-molecular-weight aggregates as evidenced by a peak containing HRF eluting in the void volume of the gel-filtration column. This possibly contributed to the difficulty in crystallizing HRF. The optical spectra of the two proteins are identical and only the spectrum of MRF is shown in Fig. 2.

3.3. Structure determination

Single crystals were grown of the native form of MRF. Attempts to obtain single large crystals of HRF were unsuccessful and yielded only rosettes and microcrystals. After attempts to locate two distinct Fe sites in data sets collected from native crystals at the Fe absorption edge failed, crystals derivatized with thimerosal were obtained. Table 1 shows the data-collection and refinement statistics for MRF. The structure of the thimerosal derivative of MRF was solved to 1.7 Å resolution using SAD and a model containing 132 of the protein's 157 residues and four ethylmercury molecules was built into the electron density, while the first 12 N-terminal residues, three residues from an extended solvent-exposed loop and the last ten C-terminal residues were missing. An additional 2.07 Å resolution data set was obtained from a native crystal. Although the phasing data set had a higher resolution, the electron density in the regions of the ethylmercury sites was poor and a significant change in the unit-cell parameters (Table 1) with respect to the native crystals suggested that the binding of the Hg atoms changed the structure of the protein. For this reason, the structure obtained for the phasing data set was used for molecular replacement against the 2.07 Å native data. Of the total of 157 residues in the native protein, 129 were fitted into electron density. The missing residues were the same residues that were absent from the mercury-derivative structure, along with one extra N-terminal residue and two residues of the extended loop, which was displaced significantly from its position in the derivatized structure. At this stage, it was apparent that extending the C-terminus by another seven residues could fill a cylinder of strong positive density clearly corresponding to protein backbone near the active site. Because the side chains in this region were very poorly resolved, there were multiple possible conformations of the C-terminus that could satisfy the electron density equally well. This density was also absent in the mercury-bound structure; in fact, the positioning of the symmetry-related protein in the adjacent asymmetric unit would preclude the placement of any residues in this location. Although these C-terminal residues were included in the deposited structure, their positioning should be considered speculative and likely to be an artefact of crystal packing. The final model contained 136 protein residues, 45 water molecules, a [2Fe–2S] iron–sulfur cluster and one molecule of ethylene glycol.

3.4. Overall fold

MRF exhibits the two-domain fold common to all Rieske proteins. The larger domain consists of a partial β-barrel made up of six antiparallel strands commonly labelled $\beta1$, $\beta2$, $\beta3$, $\beta4$,

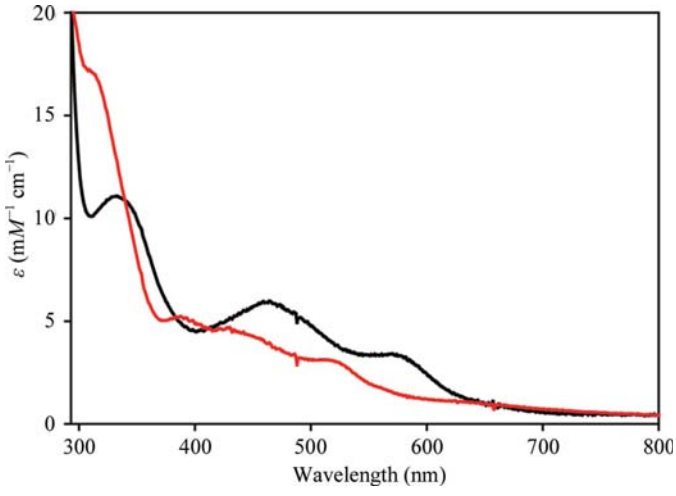

Figure 2
Electronic absorption spectra of oxidized (black line) and reduced (red line) MRF. The change in absorbance at 460 nm was monitored for reduction studies.

β9 and β10 (Fig. 3). Despite the low sequence identity, the backbone of this domain is virtually identical to those of the large domains found in the previously solved structures of BphF (Colbert *et al.*, 2000), T4moC (Moe *et al.*, 2006) and CarAc (Nam *et al.*, 2005), the ferredoxin components of biphenyl dioxygenase, toluene 4-monooxygenase and carbazole 1,9a-dioxygenase, respectively (Fig. 5*a*). The smaller cluster-binding domain is more divergent among the three proteins. This domain typically consists of a four-stranded antiparallel β-sheet (strands β5, β6, β7 and β8). The [2Fe–2S] cluster is located near the surface of the protein between the four-stranded sheet and the large domain and is primarily made up of the random coil before the β5 strand and the loop connecting β6 and β7. MRF differs from BphF and T4moC in the length of the β5 and β6 β-strands of its cluster-binding domain, which are longer and have a more pronounced right-handed twist than the bacterial ferredoxins, and in the loop following the β8 β-strand, where MRF forms a two-strand β-sheet with the βX strand five residues in length ending in disordered random coil over 14 Å away from the bulk of protein. Large loops between the β8 and β9 strands are typically found in the Rieske domains of trimeric aromatic ring dioxygenases, where the side of the loop facing the active site forms part of the interface with the adjacent subunit.

3.5. Electrostatic surface

Fig. 4 shows electrostatic surfaces of MRF (Fig. 4*a*) and T4moC (Fig. 4*b*). Arg65 of T4moC has been demonstrated to be an important determinant of binding specificity between T4moC and its electron donor, the oxidoreductase T4moF (Elsen *et al.*, manuscript in preparation). Arg65 of T4moC is the slightly basic patch in the center of the molecule. MRF has been aligned and oriented similarly. A large acidic patch is visible directly beneath Arg65 in the T4moC structure. In contrast, MRF has a near-equal mixture of basic and acidic surface area and has a net charge of −2.6 at pH 7.5 compared

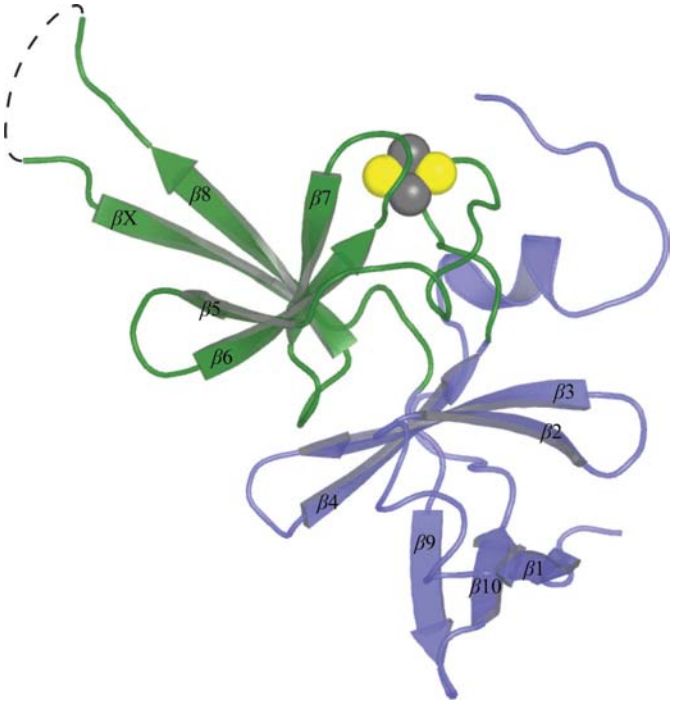

Figure 3
Ribbon representation of mouse soluble Rieske ferredoxin. The large domain is shown in blue and the cluster-binding domain in green. The iron–sulfur cluster is shown as spheres, with the S atoms colored yellow and the Fe atoms gray. The dashed line indicates the approximate location of five disordered residues in the β8–βX loop.

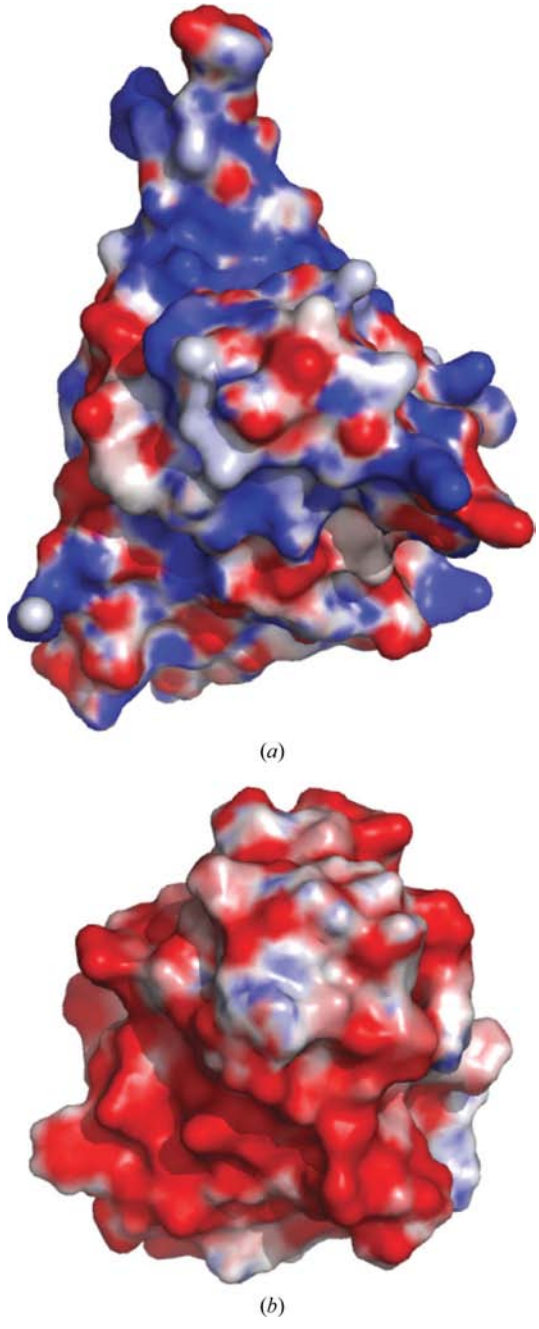

Figure 4
Electrostatic surfaces of MRF and T4moC. The structures of MRF (*a*) and T4moC (*b*) were aligned in *PyMOL* and electrostatic surfaces were computed using the *APBS Tools* plugin (Baker *et al.*, 2001) for a range from $-10kT/e$ to $10kT/e$, with basic areas in blue and acidic areas in red. Both proteins are shown in the same orientation, with the cluster-binding domain on top and the proline loop facing away from the viewer.

with −14.5 for T4moC. The extended proline loop of MRF is visible at the top of the structure. The surface of the loop facing the [2Fe–2S] cluster has significant positive charge and protrudes well above the histidine ligands. In contrast, the area surrounding the [2Fe–2S] cluster of T4moC is negatively charged and the histidine ligands are unobstructed by the proline loop. The large differences in surface charge and morphology between MRF and T4moC offer a physical basis for the low second-order rate constant for reduction of MRF by T4moF (see below). These factors, in addition to the expected difference in reduction potential between T4moC and MRF, may also explain the inability of MRF to transfer electrons to T4moH.

3.6. Iron–sulfur cluster-binding site

The architectures of the iron–sulfur cluster-binding sites in previously solved structures of Rieske-type proteins have been classified into two different types. Both types have two loops containing the C*X*H and C*XX*H motifs, which also provide many of the hydrogen bonds to the S atoms of the cluster and the ligating cysteine residues. In the first type, representing the majority of Rieske and Rieske-type proteins, a third loop containing a highly conserved proline residue interacts with the S1 atom of the iron–sulfur cluster, protecting it from the solvent. In the second type, which includes the ferredoxin components of monooxygenase complexes (Moe *et al.*, 2006) and the oxygenase components of dioxygenase complexes (Dong *et al.*, 2005; Friemann *et al.*, 2005; Furusawa *et al.*, 2004; Kauppi *et al.*, 1998; Nojiri *et al.*, 2005) and some monooxygenases (Martins *et al.*, 2005), this third loop is highly variable in length and sequence and is displaced away from the active site by the side chain of an aromatic residue located two residues after the C*XX*H motif. The aromatic side chain, which is frequently a tryptophan, takes the place of the conserved proline and sits with one face adjacent to the S1 atom of the iron–sulfur cluster. The active site of MRF falls into this latter category and provides the first example of a tyrosine residue taking the place of the conserved proline. The tyrosine ring lies roughly perpendicular to the plane of the iron–sulfur cluster, with the ring atoms located 3.6–4.9 Å away from the S1 atom.

Fig. 5(*b*) shows the structure of MRF near the [2Fe–2S] cluster. The cluster is coordinated by residues His59 and His83 at the Fe1 atom and residues Cys57 and Cys80 at the Fe2 atom. The geometry of the cluster is consistent within error with previous high-resolution structures of Rieske proteins (Hunsicker-Wang *et al.*, 2003; Bonisch *et al.*, 2002). Based on the criteria for identifying a hydrogen bond used by Hunsicker-Wang *et al.* (2003), *i.e.* a distance between the electron donor and acceptor of not more than 3.8 Å and an angle formed by the donor, acceptor and heavy atom of not less than 120°, the four S atoms participate in a total of six hydrogen bonds with the backbone amide H atoms of the surrounding residues (Fig. 5*b*). Both of the cluster S atoms are hydrogen bonded by two residues: S2 by Ser60 and Gly62, and S1 by His83 and Tyr85. The S atoms of the ligating cysteines each form one hydrogen bond; specifically, His59 hydrogen bonds to the S atom of Cys57 and Trp82 to the S atom of Cys80. The arrangement of bonds is roughly symmetric about the cluster's twofold rotational axis.

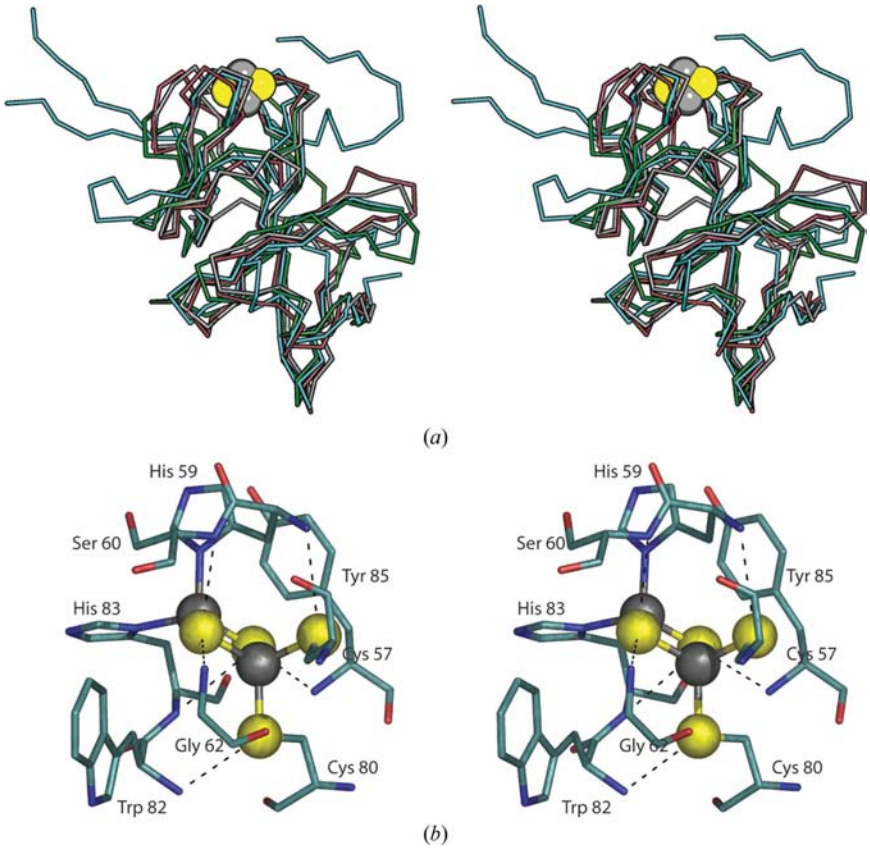

Figure 5
Comparison of Rieske ferredoxin folds and the MRF active site. (*a*) Stereo image of the alignment of MRF (cyan), BphF (PDB code 1fqt, gray), T4moC (PDB code 1vm9, green) and CarAc (PDB code 1vck, red). The positioning of the space-filling representation of the iron–sulfur cluster corresponds to its location in the MRF structure. (*b*) Stereo image of the MRF active site and residues participating in hydrogen bonding to the atoms of the iron–sulfur cluster and the cysteine S atoms, which are represented as spheres.

The [2Fe–2S] centers of Rieske proteins exhibit a broad spectrum of redox potentials ranging between −167 and +490 mV (Schmidt & Shaw, 2001). Hunsicker-Wang and coworkers have shown a strong correlation between the number and nature of hydrogen bonds to the S atoms of the cluster and the coordinating cysteine residues, with stronger more numerous bonds stabilizing the reduced state and thus increasing the redox potential. Also, the presence of an aromatic residue located two residues after the C*XX*H motif has been proposed to

lower the redox potential by placing the electron density from the aromatic side chain adjacent to the [2Fe–2S] center (Elsen *et al.*, 2007). MRF's total of six hydrogen bonds to the cluster and its coordinating cysteines is higher than that observed for previously solved structures of the ferredoxin components of bacterial ROs. For example, T4moC, BphF and CarAc have five, three and two active-site hydrogen bonds and redox potentials of −173, −157 and −169 mV, respectively (Elsen *et al.*, 2007). However, the presence of Tyr85 adjacent to the [2Fe–2S] center of MRF may partially offset the effect of the additional hydrogen bonds. MRF is predicted to have a redox potential that is slightly more positive than those of the soluble Rieske-type ferredoxins mentioned.

3.7. Chemical and enzymatic reduction of MRF

MRF was readily reduced by sodium dithionite (Fig. 2). It was also found that MRF could be enzymatically reduced by both prokaryotic and eukaryotic oxidoreductases but with significantly different rates. The rate of reduction of MRF by the bacterial oxidoreductase T4moF (Bailey *et al.*, 2007) was measured at multiple MRF concentrations in the presence of saturating NADH. The rate increased linearly with MRF concentration up to 100 μM, corresponding to an observed second-order rate of 0.2 $\mu M^{-1}\,s^{-1}$, and the apparent K_M between T4moF and MRF had a lower limit of $\sim$100 μM. In comparison, the biological electron-transfer partner for T4moF, the Rieske-type ferredoxin T4moC, was reduced at >200 s^{-1} with an apparent K_M of less than 5 μM, giving a second-order rate constant of >40 $\mu M^{-1}\,s^{-1}$ (Elsen *et al.*, manuscript in preparation).

MRF could also be reduced by the eukaryotic oxidoreductase ferredoxin NADPH reductase (FdR) from *Zea mays* (Ritchie *et al.*, 1994), although at a significantly slower rate (<0.001 $\mu M^{-1}\,s^{-1}$). Considering the biological electron-transfer partners of T4moF (T4moC, a Rieske-type ferredoxin) and FdR (a plant-type ferredoxin), it is perhaps not surprising that the bacterial oxidoreductase reduces MRF more efficiently.

T4moF and FdR could also reduce HRF. A second-order rate constant for reduction by T4moF was not calculated; however, at 50 μM HRF the reduction rate was similar to that of MRF and FdR reduced HRF very slowly. After reduction, exposure to air returned both MRF and HRF to the oxidized state and gave optical spectra that were identical to those of the as-isolated proteins. This indicates that the formation of reactive oxygen species such as superoxide does not damage the [2Fe–2S] cluster of these ferredoxins.

Despite its capacity to be reduced by T4moF, neither MRF nor HRF stimulated *p*-cresol formation when substituted for T4moC in the T4MO complex. The inability of these Rieske proteins to transfer electrons to T4moH is either a consequence of a high reduction potential, as suggested by the hydrogen-bonding pattern, or an inability to form an efficient electron-transfer complex. Indeed, even BphF, which has a redox potential similar to that of T4moC and is more closely related structurally, could not stimulate *p*-cresol formation, indicating that a specific protein–protein interaction between T4moH and its Rieske-type ferredoxin electron donor is required for electron transfer (Elsen *et al.*, 2007).

3.8. Possible biological function

The biological electron-transfer partners of Rieske proteins and Rieske-type ferredoxins include hemes (Link & Iwata, 1996), diiron clusters (Pikus *et al.*, 1996), mononuclear iron centers ligated by the 2-His-1-carboxylate facial triad (Kauppi *et al.*, 1998) and [3Fe–4S]/molybdenum cofactors (Ellis *et al.*, 2001). They are found as membrane-bound subunits (Carrell *et al.*, 1997), as domains of larger oxidase complexes (Kauppi *et al.*, 1998), as subunits in the $\alpha_2\beta_2$ arsenite oxidase (Ellis *et al.*, 2001) and as soluble monomeric ferredoxins (Moe *et al.*, 2006). The extended Pro-loop of MRF is most similar to the extended Pro-loops found in the Rieske domains of the Rieske dioxygenases. In NDO, this loop provides an extended interface with the adjacent subunit and thus helps to stabilize the trimeric quaternary structure and also orient the [2Fe–2S] cluster to form an active site that crosses subunit boundaries. The presence of the extended loop in MRF supports the likelihood that the protein also undergoes strong and likely specific interactions with a presently unknown eukaryotic electron acceptor. A strong affinity for its electron-transfer partner may facilitate its identification by pull-down methods using the affinity-tagged MRF.

This work was funded by the National Institutes of Health Protein Structure Initiative grant U54 GM074901 (GNP and EJL), National Science Foundation grant MCB-0316232 (BGF and NLE), National Library of Medicine grant 5T15LM007359 (EJL) and NHGRI training grant 5T32HG002760 (JGM). The authors would like to thank Russell Wrobel for providing the plasmids containing the MRF gene.

References

Adams, P. D., Grosse-Kunstleve, R. W., Hung, L.-W., Ioerger, T. R., McCoy, A. J., Moriarty, N. W., Read, R. J., Sacchettini, J. C., Sauter, N. K. & Terwilliger, T. C. (2002). *Acta Cryst.* D**58**, 1948–1954.

Bailey, L. J., Elsen, N. L., Pierce, B. S. & Fox, B. G. (2007). *Protein Expr. Purif.* **57**, 9–16.

Baker, N. A., Sept, D., Joseph, S., Holst, M. J. & McCammon, J. A. (2001). *Proc. Natl Acad. Sci. USA*, **98**, 10037–10041.

Bonisch, H., Schmidt, C. L., Schafer, G. & Ladenstein, R. (2002). *J. Mol. Biol.* **319**, 791–805.

Carrell, C. J., Zhang, H., Cramer, W. A. & Smith, J. L. (1997). *Structure*, **5**, 1613–1625.

Clewley, J. P. & Arnold, C. (1997). *Methods Mol. Biol.* **70**, 119–129.

Cohen, S. X., Morris, R. J., Fernandez, F. J., Ben Jelloul, M., Kakaris, M., Parthasarathy, V., Lamzin, V. S., Kleywegt, G. J. & Perrakis, A. (2004). *Acta Cryst.* D**60**, 2222–2229.

Colbert, C. L., Couture, M. M., Eltis, L. D. & Bolin, J. T. (2000). *Structure*, **8**, 1267–1278.

Davis, I. W., Leaver-Fay, A., Chen, V. B., Block, J. N., Kapral, G. J., Wang, X., Murray, L. W., Arendall, W. B. III, Snoeyink, J., Richardson, J. S. & Richardson, D. C. (2007). *Nucleic Acids Res.* **35**, W375–W383.

Dong, X., Fushinobu, S., Fukuda, E., Terada, T., Nakamura, S., Shimizu, K., Nojiri, H., Omori, T., Shoun, H. & Wakagi, T. (2005). *J. Bacteriol.* **187**, 2483–2490.
Ellis, P. J., Conrads, T., Hille, R. & Kuhn, P. (2001). *Structure*, **9**, 125–132.
Elsen, N. L., Moe, L. A., McMartin, L. A. & Fox, B. G. (2007). *Biochemistry*, **46**, 976–986.
Emsley, P. & Cowtan, K. (2004). *Acta Cryst.* D**60**, 2126–2132.
Fee, J. A., Findling, K. L., Yoshida, T., Hille, R., Tarr, G. E., Hearshen, D. O., Dunham, W. R., Day, E. P., Kent, T. A. & Münck, E. (1984). *J. Biol. Chem.* **259**, 124–133.
Ferraro, D. J., Gakhar, L. & Ramaswamy, S. (2005). *Biochem. Biophys. Res. Commun.* **338**, 175–190.
Fischer, D. S. & Price, D. C. (1964). *Clin. Chem.* **10**, 21–31.
Friemann, R., Ivkovic Jensen, M. M., Lessner, D. J., Yu, C. L., Gibson, D. T., Parales, R. E., Eklund, H. & Ramaswamy, S. (2005). *J. Mol. Biol.* **348**, 1139–1151.
Furusawa, Y., Nagarajan, V., Tanokura, M., Masai, E., Fukuda, M. & Senda, T. (2004). *J. Mol. Biol.* **342**, 1041–1052.
Hunsicker-Wang, L. M., Heine, A., Chen, Y., Luna, E. P., Todaro, T., Zhang, Y. M., Williams, P. A., McRee, D. E., Hirst, J., Stout, C. D. & Fee, J. A. (2003). *Biochemistry*, **42**, 7303–7317.
Iwata, S., Saynovits, M., Link, T. A. & Michel, H. (1996). *Structure*, **4**, 567–579.
Kauppi, B., Lee, K., Carredano, E., Parales, R. E., Gibson, D. T., Eklund, H. & Ramaswamy, S. (1998). *Structure*, **6**, 571–586.
Leahy, J. G., Batchelor, P. J. & Morcomb, S. M. (2003). *FEMS Microbiol. Rev.* **27**, 449–479.
Link, T. A. & Iwata, S. (1996). *Biochim. Biophys. Acta*, **1275**, 54–60.
Lledo, B., Martinez-Espinosa, R. M., Marhuenda-Egea, F. C. & Bonete, M. J. (2004). *Biochim. Biophys. Acta*, **1674**, 50–59.
Martins, B. M., Svetlitchnaia, T. & Dobbek, H. (2005). *Structure*, **13**, 817–824.
Moe, L. A., Bingman, C. A., Wesenberg, G. E., Phillips, G. N. & Fox, B. G. (2006). *Acta Cryst.* D**62**, 476–482.
Murshudov, G. N., Vagin, A. A. & Dodson, E. J. (1997). *Acta Cryst.* D**53**, 240–255.
Nam, J. W., Noguchi, H., Fujimoto, Z., Mizuno, H., Ashikawa, Y., Abo, M., Fushinobu, S., Kobashi, N., Wakagi, T., Iwata, K., Yoshida, T., Habe, H., Yamane, H., Omori, T. & Nojiri, H. (2005). *Proteins*, **58**, 779–789.
Nojiri, H., Ashikawa, Y., Noguchi, H., Nam, J. W., Urata, M., Fujimoto, Z., Uchimura, H., Terada, T., Nakamura, S., Shimizu, K., Yoshida, T., Habe, H. & Omori, T. (2005). *J. Mol. Biol.* **351**, 355–370.
Otwinowski, Z. & Minor, W. (1997). *Methods Enzymol.* **276**, 207–326.
Painter, J. & Merritt, E. A. (2006). *Acta Cryst.* D**62**, 439–450.
Pikus, J. D., Studts, J. M., Achim, C., Kauffmann, K. E., Münck, E., Steffan, R. J., McClay, K. & Fox, B. G. (1996). *Biochemistry*, **35**, 9106–9119.
Rieske, J. S. (1968). *J. Biol. Chem.* **239**, 3017–3022.
Ritchie, S. W., Redinbaugh, M. G., Shiraishi, N., Vrba, J. M. & Campbell, W. H. (1994). *Plant Mol. Biol.* **26**, 679–690.
Schafer, G., Purschke, W. G., Gleissner, M. & Schmidt, C. L. (1996). *Biochim. Biophys. Acta*, **1275**, 16–20.
Schlenzka, W., Shaw, L., Kelm, S., Schmidt, C. L., Bill, E., Trautwein, A. X., Lottspeich, F. & Schauer, R. (1996). *FEBS Lett.* **385**, 197–200.
Schmidt, C. L. & Shaw, L. (2001). *J. Bioenerg. Biomembr.* **33**, 9–26.
Sharff, A. J., Rodseth, L. E., Spurlino, J. C. & Quiocho, F. A. (1992). *Biochemistry*, **31**, 10657–10663.
Sheldrick, G. M. (2008). *Acta Cryst.* A**64**, 112–122.
Thao, S., Zhao, Q., Kimball, T., Steffen, E., Blommel, P. G., Riters, M., Newman, C. S., Fox, B. G. & Wrobel, R. L. (2004). *J. Struct. Funct. Genomics*, **5**, 267–276.
Trumpower, B. L. & Gennis, R. B. (1994). *Annu. Rev. Biochem.* **63**, 675–716.
Vagin, A. & Teplyakov, A. (1997). *J. Appl. Cryst.* **30**, 1022–1025.
Vonrhein, C., Blanc, E., Roversi, P. & Bricogne, G. (2006). *Methods Mol. Biol.* **364**, 215–230.
Winn, M. D., Isupov, M. N. & Murshudov, G. N. (2001). *Acta Cryst.* D**57**, 122–133.
Xie, Q., Lin, T., Zhang, Y., Zheng, J. & Bonanno, J. A. (2005). *J. Biol. Chem.* **280**, 19673–19681.